PHYSICAL REVIEW MATERIALS **7**, 054405 (2023)

Spin-polarized two-dimensional electron/hole gas at the interface of nonmagnetic semiconducting half-Heusler compounds: Modified Slater-Pauling rule for half-metallicity at the interface

Emel Gürbüz,[1] Sukanya Ghosh,[1] Ersoy Şaşıoğlu,[2,*] Iosif Galanakis,[3,†] Ingrid Mertig,[2] and Biplab Sanyal[1,‡]
[1]*Department of Physics and Astronomy, Uppsala University, 75120 Uppsala, Sweden*
[2]*Institute of Physics, Martin Luther University Halle-Wittenberg, 06120 Halle (Saale), Germany*
[3]*Department of Materials Science, School of Natural Sciences, University of Patras, GR-26504 Patra, Greece*

(Received 3 February 2023; revised 25 April 2023; accepted 12 May 2023; published 30 May 2023)

Half-Heusler compounds with 18 valence electrons per unit cell are well-known nonmagnetic semiconductors. Employing first-principles electronic band-structure calculations, we study the interface properties of the half-Heusler heterojunctions based on FeVSb, CoTiSb, CoVSn, and NiTiSn compounds, which belong to this category of materials. Our results show that several of these heterojunction interfaces become not only metallic but also magnetic. The emergence of spin-polarization is accompanied by the formation of two-dimensional electron gas or hole gas at the interface. A qualitative analysis of the origin of the spin polarization at the interfaces suggests that strong correlations are responsible. For the cases of magnetic interfaces where half-metallicity is also present, we propose a modified Slater-Pauling rule similar to the one for bulk half-metallic half-Heusler compounds. Additionally, we calculate exchange parameters, Curie temperatures, and magnetic anisotropy energies for magnetic interfaces. Our study, along with recent experimental evidence confirming the presence of two-dimensional electron gas at CoTiSb/NiTiSn heterojunctions, may motivate future efforts to explore and realize device applications using these heterojunctions.

DOI: 10.1103/PhysRevMaterials.7.054405

I. INTRODUCTION

Heusler compounds, named after Fritz Heusler [1,2], are ternary and quaternary intermetallic compounds that crystallize in close-packed lattice structures [3–5]. In particular, the discovery of half-metallicity (the electronic band structure is metallic for one spin channel and semiconducting for the other [6]) in Heusler compounds, which was followed by other exotic behaviors like spin-gapless semiconductors and spin-filter materials [7], led to the proposal of novel devices [8–12]. An important role in the rapid growth of this research field was played by first-principles electronic band-structure calculations. On the one hand, they successfully explained the origin of half-metallicity and linked it to the magnetic properties through the so-called Slater-Pauling rules [13–18], and on the other hand, extended databases built using such calculations resulted in the prediction of hundreds of new Heusler compounds that were later grown experimentally [19–26].

Heusler compounds are categorized into various families depending on the number of atoms in the unit cell and their ordering [3,4]. The ones with the chemical formula XYZ, where X and Y are transition-metal atoms and Z is a metalloid, are named half-Heusler (or semi-Heusler) compounds. When the number of valence electrons in the unit cell exceeds 19 and goes up to 22, most of them are half-metals [13]. As shown by Galanakis *et al.*, the half-metallicity is directly connected to the total spin magnetic moment through the Slater-Pauling rule $M_t = Z_t - 18$, where M_t is the total spin magnetic moment in the unit cell expressed in μ_B, and Z_t is the total number of valence electrons in the unit cell. The number 18 expresses the fact that there are exactly nine occupied states in the minority-spin electronic band structure, which exhibits semiconducting behavior. There is a single *s* and a triple *p* band low in energy stemming from the Z atom. The *d* valence orbitals of the X and Y atoms hybridize creating five occupied bonding orbitals, which are separated by an energy gap from the five unoccupied antibonding orbitals.

The Slater-Pauling rule correctly predicts that half-Heusler compounds with exactly 18 valence electrons should be nonmagnetic semiconductors with a gap in both spin-channels [13]. This "18-electron rule" for semiconducting half-Heusler compounds was also derived by Jung *et al.* based on ionic arguments [27]. Among the 18-valence-electron half-Heusler compounds, CoTiSb, NiTiSn, FeVSb, and CoVSn have attracted most of the attention. Pierre and collaborators confirmed experimentally the nonmagnetic semiconducting character of NiTiSn [28]. Tobola *et al.* have shown experimentally that CoTiSb is also a nonmagnetic semiconductor [29]. The experimental findings for both NiTiSn and CoTiSb have also been confirmed by *ab initio* calculations in Ref. [29]. Recently, Ouardi *et al.* synthesized CoTiSb and investigated it both theoretically and experimentally [30]. Lue and collaborators grew samples of CoVSn, and their findings were consistent with a nonmagnetic semiconducting behavior [31]. Finally, Mokhtari and collaborators have shown theoretically that FeVSb is also a nonmagnetic semiconductor [32], followed by the experimental observation by Shourov

---

[*] ersoy.sasioglu@physik.uni-halle.de

[†] galanakis@upatras.gr

[‡] biplab.sanyal@physics.uu.se

et al. [33]. Ma *et al.* studied using first-principles calculations a total of 378 half-Heusler compounds [19]. Among them, there were 27 compounds with 18 valence electrons, including the aforementioned ones, which were all found to be nonmagnetic semiconductors [19]. Doping these compounds with transition-metal atoms [34–42] or vacancies [43] leads to a half-metallic behavior.

Recently, Sharan *et al.*, employing *ab initio* calculations, studied the formation of a two-dimensional electron gas (2DEG) or hole gas (2DHG) at the interface between CoTiSb and NiTiSn compounds [44]. To model the heterojunction, they assumed a superlattice along the [001] direction. Along the [001] direction, CoTiSb is nonpolar and NiTiSn is polar [44]. Similarly to the complex oxides' polar/nonpolar interfaces [45–47], a 2DEG is formed at the (TiSb)-Ni interface while a 2DHG is formed at the Co-(TiSn) interface [44]. A 2DEG (2DHG) is a type of electronic system in which a large number of electrons (holes) are confined to a very thin, two-dimensional layer like the one occurring at an interface of a heterojunction. Electrons (holes) are free to move in the two dimensions, but they are strongly confined in the third dimension leading to many potential applications, including high-speed electronic devices and quantum computers [48]. We should note here that usually the two-dimensional electron gas in the case of surfaces is referred to as "2D electron liquid" [49]. Experimentally, Harrington has grown heterostructures made up of alternating 25-nm-thick CoTiSb and NiTiSn [50]. Although the structure of the interface has not been studied, interface transport measurements suggest that 2DEG is present at the interface giving indirect evidence for its formation [50]. The characterization of Heusler interfaces is a hard task, and in our opinion no concluding results exist. But as discussed in a recent article by Kawasaki entitled "Heusler interfaces—Opportunities beyond spintronics?" the manipulation of Heusler interfaces with a variety of other materials will lead to exciting new phenomena [10].

The goal of this study is to provide a comprehensive understanding of the electronic and magnetic properties of interfaces formed by various combinations of CoTiSb, NiTiSn, FeVSn, and CoVSn nonmagnetic semiconducting Heusler compounds along the [001] growth direction by employing state-of-the-art first-principles electronic band-structure calculations. We find that for all heterojunctions except for CoTiSb/CoVSn, the emergence of 2DEG or 2DHG at the interfaces is accompanied by the occurrence of magnetism. We qualitatively discuss the origin of interface magnetism on the basis of the Stoner model. In some cases, our calculations suggest that also half-metallicity is present, and we formulate a modified version of the Slater-Pauling rule to connect the magnetic properties to half-metallicity and the total number of valence electrons at the specific interface. Finally, we present the exchange constants for the magnetic interfaces, and we use them to predict the Curie temperature, which is important for applications. We should mention at this point that according to the Mermin-Wagner theorem, the long-range magnetic order does not exist in one-(1D) or two-dimensional (2D) isotropic magnets. But as shown recently in Ref. [51], short-range exchange interactions even in the absence of magnetic anisotropy can induce magnetic order in finite-size 2D magnets even for samples of millimeters size. Thus, the magnetic interfaces discussed in the present study are feasible and can be realized in realistic spintronic devices. The rest of the manuscript is organized as follows: In Sec. II we present details of our calculations, in Sec. III we present our results, and finally in Sec. IV we summarize our results and present the conclusions of our study.

TABLE I. Equilibrium lattice parameters (a) taken from Ref. [19], number of valence electrons per unit cell (Z_t), and energy band gap E_{gap} for FeVSb, CoTiSb, CoVSn, and NiTiSn half-Heusler compounds.

Compound	a (Å)	Z_t	E_{gap} (eV)
FeVSb	5.78	18	0.34
CoTiSb	5.88	18	1.09
CoVSn	5.79	18	0.63
NiTiSn	5.93	18	0.47

II. COMPUTATIONAL METHOD

The bulk half-Heusler compounds XYZ crystallize in the cubic $C1_b$ lattice structures shown in the upper panel of Fig. 1(a). The space group is the $F\bar{4}3m$ and actually consists of four interpenetrating fcc sublattices; one is empty and the other three are occupied by the X, Y, and Z atoms. The unit cell is a fcc one with three atoms as a basis along the long diagonal of the cube: X at (0 0 0), Y at $(\frac{1}{4}\,\frac{1}{4}\,\frac{1}{4})$, and Z at $(\frac{3}{4}\,\frac{3}{4}\,\frac{3}{4})$ in Wyckoff coordinates. The cube presented in the figure contains exactly four unit cells. In our interface calculations, we need a supercell along the [001] direction. To construct the simulation cell for the supercell calculations, we do not need to use the bulk cube as the basis for the construction, but the tetragonal cell presented in the lower part of Fig. 1(a) is sufficient. This tetragonal cell has half the volume of the cube and contains two unit cells. Along the [001] direction, the consecutive layers are made up of pure X and mixed YZ layers and the in-plane lattice parameter equals the $\frac{1}{\sqrt{2}}$ of the cube's lattice parameter. For all four compounds FeVSb, CoTiSb, CoVSn, and NiTiSn, we adopted the equilibrium lattice parameters calculated in Ref. [19] using the Vienna Ab-initio Simulation Package (VASP) [52,53] in conjunction with the generalized gradient approximation (GGA) to the exchange-correlation potential [54]. We present the lattice parameters of the bulk compounds adopted in our study in Table I.

To carry out the spin-polarized density functional theory (DFT) calculations, we employ the QUANTUMATK software package [55,56]. We use linear combinations of atomic orbitals (LCAO) as a basis set together with norm-conserving PseudoDojo pseudopotentials [57] with the Perdew-Burke-Ernzerhof (PBE) parametrization of the GGA functional [54]. For the determination of the ground-state properties of the bulk compounds, we use a 15×15×15 Monkhorst-Pack **k**-point grid, while for periodic supercell calculations a 20×20×2 Monkhorst-Pack **k**-point grid is adopted [58].

When we form heterojunctions using FeVSb, CoTiSb, CoVSn, and NiTiSn compounds, we get six possible combinations, and for each combination there are two possible

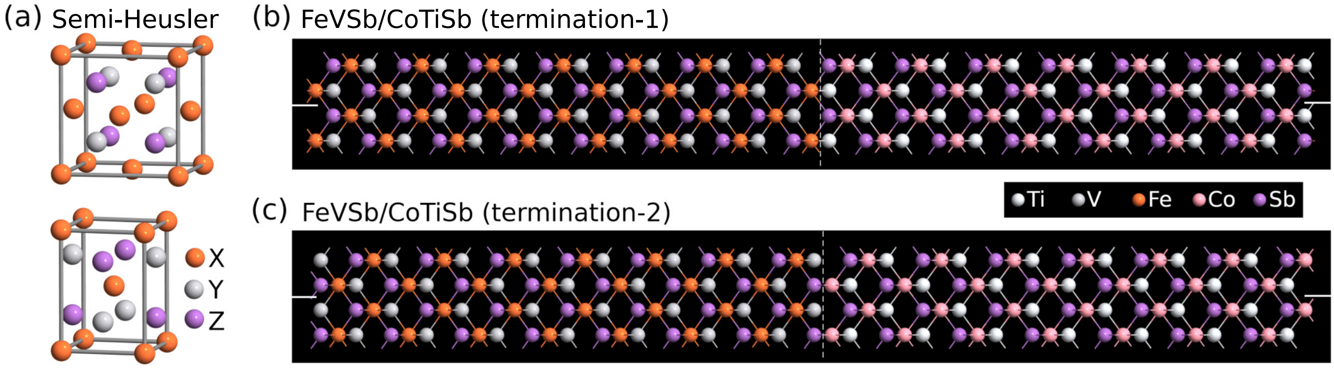

FIG. 1. (a) Upper panel: Schematic representation of the conventional cubic cell of XYZ half-Heusler compounds. Lower panel: Minimal bulk tetragonal unit cell used to construct the simulation cell for the superlattice calculations (see the text for details). (b) and (c) Cross-section views along the (100) plane of the superlattice structure for the two different possible interface terminations in the case of the FeVSb/CoTiSb heterojunction, using the twice repeated tetragonal bulk cell as the basis.

interface terminations, denoted as Termination-1 and Termination-2 in Table III and shown in Fig. 1 using FeVSb/CoTiSb as an example (the two possible interfaces are made up of Fe-TiSb and VSb-Co layers, respectively). If one of the two interface terminations generates a 2DEG, the other will be 2DHG, as we will discuss in the next section. To simulate the heterojunction, we assume a supercell consisting of 29 (27) layers of FeVSb and 27 (29) layers of CoTiSb for the first (second) termination. We construct the simulation supercell by stacking the tetragonal unit cell presented in the lower panel of Fig. 1(a) along the out-of-plane direction. Specifically, our heterojunctions are formed by a 14-fold repetition of the tetragonal Heusler unit cell with the atoms assigned to the atomic planes as described below, giving a supercell of 42 atomic planes containing in total 84 atoms. To construct the supercell, we fix for the first material, for instance in the FeVSb/CoTiSb supercell, the lattice parameter of FeVSb is the cubic one shown in Table I. For the second compound, CoTiSb in our example, we consider as an in-plane lattice parameter the one of FeVSb, and we relax the out-of-plane lattice parameter along the [001] direction; in Table II we present the c/a ratio for the second compound of the heterostructure in the supercell. We expect that our choice of lattice parameters for the two Heusler compounds only marginally affects the calculated results. The maximum difference in the lattice constants between the four bulk compounds is 2.5%, and as shown by Block and collaborators, moderate values of tetragonalization do not alter significantly the properties of Heusler compounds [59]. In Table II we also provide the relative stability energy E_s, which is the energy difference between the two interfaces using device-type calculations. In each case, we set the energy of the termination with the larger total energy as zero, and thus the one with the negative E_s is the most stable. There is no clear trend in which one of the two terminations is more stable and the results are heterojunction-dependent. We should note here that in device-type calculations, contrary to the supercell approach, we have exactly the same number of atoms in the scattering region as well as in electrodes and thus we can compare the energy of the two different terminations.

In the present study, we adopted the supercell approach instead of a two-terminal device model implemented in QuantumATK and adopted in previous studies [8,9,11,12] since the band-structure calculations using the device model are computationally extremely demanding. For FeVSb/NiTiSn heterojunction, we performed also calculations using the device model with two semi-infinite leads by employing the nonequilibrium Green's function (NEFG) approach combined with DFT. For these DFT+NEGF calculations, we used a 20×20×115 **k**-point mesh. The results were identical to the ones obtained by the supercell approach and thus the use of the latter is completely justified.

To study finite-temperature properties of the interfaces, we map the complex multi-sublattice itinerant electron problem onto a classical effective Heisenberg Hamiltonian

$$H_\mathrm{eff} = -\sum_{\mathrm{i,j}}\sum_{\mu,\nu} J_{\mathrm{ij}}^{\mu\nu}\boldsymbol{S}_i^{\mu}\cdot\boldsymbol{S}_j^{\nu}, \tag{1}$$

where μ and ν denote different sublattices at the interface, i and j indicate atomic positions, and $\boldsymbol{S}_i^{\mu}$ is the unit vector of the i site in the μ sublattice. The Heisenberg exchange constants $J_{\mathrm{ij}}^{\mu\nu}$ are calculated by employing the Liechtenstein formalism [60] within the full-potential linear muffin-tin orbital (FP-LMTO) code RSPt [61]. The crystalline structure information for the studied interfaces obtained with the LCAO is used as input for the electronic structure calculations by the FP-LMTO approach. According to our tests, both QuantumATK and FP-LMTO methods provide a very similar electronic structure for the systems under study.

To estimate the Curie temperature T_C of the magnetic interfaces, we use the mean-field approximation for a multi-sublattice system [62–64], which is given by

$$T_C = \frac{2}{3k_B}J_\mathrm{L}^{\mu\nu}, \tag{2}$$

where $J_\mathrm{L}^{\mu\nu}$ is the largest eigenvalue of $J_0^{\mu\nu} = \sum_j J_{0\mathrm{j}}^{\mu\nu}$. Note that in the calculation of the Curie temperature, we take into account exchange interactions between atoms at layers around the interface which have a spin magnetic moment magnitude per layer exceeding $0.1\mu_\mathrm{B}$.

TABLE II. Six possible half-Heusler heterojunctions made up of the four considered compounds. The c/a ratios are provided for the second half-Heusler compound in the heterojunction. $E_{\rm s}$ stands for the relative stability energy of the two possible terminations for each studied heterojunction (the negative value corresponds to the most stable interface, and the zero value to the less stable one). For each studied interface, we provide the calculated atomic spin magnetic moments for the transition-metal atoms at the two interface layers: $M_{\rm X}$ stands for the transition-metal atom at the left interface layer, and $M_{\rm Y}$ denotes the transition-metal atom at the right interface layer. We also present the calculated total spin magnetic moments $M_{\rm t}^{\rm Interface}$ at the interface, taking into account the two interface layers, the ideal value for half-metallicity predicted by the $M_{\rm t}^{\rm SP} = \frac{Z_{\rm t}}{2} - 9$ Slater-Pauling rule, and the total spin magnetic moment $M_{\rm t}^{\rm Cell}$ in the simulation unit cell used for the calculations. Column 2DEG describes the character of each interface termination with respect to the two-dimensional electron gas (2DEG). SPHG stands for spin-polarized hole gas, HG for hole gas, SPEG for spin-polarized electron gas, and EG for electron gas. The last column contains the spin-polarization values at the Fermi level (see the text for the definition).

Semi-Heusler heterojunction	c/a	Interface termination	$E_{\rm s}$ (eV)	Interface composition	$Z_{\rm t}$	$M_{\rm X}$ ($\mu_{\rm B}$)	$M_{\rm Y}$ ($\mu_{\rm B}$)	$M_{\rm t}^{\rm Interface}$ ($\mu_{\rm B}$)	$M_{\rm t}^{\rm SP}$ ($\mu_{\rm B}$)	$M_{\rm t}^{\rm Cell}$ ($\mu_{\rm B}$)	2DEG	SP (%)
FeVSb/CoTiSb	1.03	T-1	0.00	Fe|TiSb	17	−0.49	0.08	−0.42	−0.5	−0.36	SPHG	67
		T-2	−0.17	VSb|Co	19	−0.10	0.76	0.64	0.5	0.43	SPEG	75
FeVSb/CoVSn	1.01	T-1	−0.57	Fe|VSn	17	−0.81	0.29	−0.54	−0.5	−0.46	SPHG	100
		T-2	0.00	VSb|Co	19	−0.03	0.18	0.15	0.5	0.09	SPEG	12
FeVSb/NiTiSn	1.05	T-1	−0.21	Fe|TiSn	16	−1.12	0.17	−0.99	−1.0	−0.90	SPHG	74
		T-2	0.00	VSb|Ni	20	0.01	1.26	1.23	1.0	0.85	SPEG	43
CoTiSb/CoVSn	0.98	T-1	−0.42	Co|VSn	18	0.00	0.00	0.00	0.0	0.00		
		T-2	0.00	TiSb|Co	18	0.00	0.00	0.00	0.0	0.00		
CoTiSb/NiTiSn	1.02	T-1	−0.18	Co|TiSn	17	0.00	0.00	0.00	−0.5	0.00	HG	0
		T-2	0.00	TiSb|Ni	19	0.00	0.00	0.00	0.5	0.00	EG	0
CoVSn/NiTiSn	1.05	T-1	0.00	Co|TiSn	17	0.00	0.00	0.00	−0.5	0.00	HG	0
		T-2	−0.66	VSn|Ni	19	−0.01	0.58	0.53	0.5	0.37	SPEG	71

III. RESULTS AND DISCUSSION

Prior to presenting our results, we should comment on our choice to use PBE, which is a GGA functional in our study. GGA functionals are well known to underestimate the band gap of semiconductors, and in this regard, more elaborated functionals like the hybrid ones, which are much more demanding in computer sources, have been developed. The latter are semiempirical combining the exact Hartree-Fock exchange with the GGA and accurately reproducing the energy band gaps in usual semiconductors [65]. In Ref. [44], the authors employed such a hybrid functional, the so-called Heyd, Scuseria, and Ernzerhof hybrid functional (HSE06) [66,67] as implemented in the VASP code [52,53]. They calculated for NiTiSn an energy band gap of 0.65 eV and for CoTiSb a value of 1.45 eV. These values are considerably larger than the 0.44 and 1.06 eV, respectively, calculated using PBE in Ref. [19] (as we will later discuss, our PBE values are in excellent agreement with these values, although we used a different electronic structure code). But, Sharan and collaborators have ignored that Heusler compounds like CoTiSb and NiTiSn are not usual semiconductors since they contain transition-metal atoms and thus the accuracy of the semiempirical hybrid functionals is not granted [44].

To clarify the above point, we have to compare the above *ab initio* calculations with experimental results. In Ref. [30], Ouardi and collaborators have determined the energy band gap of CoTiSb both experimentally as well as using *ab initio* calculations employing the PBE functional. Their calculations have shown that CoTiSb exhibits an indirect gap of 1.06 eV, identical to the PBE-derived value in Ref. [19], in excellent agreement with their experimental value of about 1.0 eV. Moreover, calculations produced an optical gap (direct gap at the Γ point) of 1.83 eV also in perfect agreement with the experimental value of 1.8 eV. Finally, the experimentally determined lattice constant was 5.884 Å in perfect agreement with their own PBE calculations as well as the PBE calculations in Ref. [19]. Thus, one can safely conclude that the PBE functional is the appropriate one to study semiconductors like the half-Heusler compounds under study, and the semiempirical hybrid functionals overestimate the band gap in these materials. Moreover, as was shown in the case of transition-metal-based full-Heusler semiconductors, many-body correlations calculated using the *GW* approximation have minimal effect on the PBE calculated electronic band structure, and the energy gaps increase by less than 0.2 eV in all cases [68]. We should finally note that, as shown in Ref. [69], the use of the more elaborated meta-GGA functionals for semiconductors leads to energy gaps that are less accurate with respect to the PBE calculated ones when compared to experimental data.

A. Electronic structure of bulk semiconducting half-Heusler compounds

The starting point of our study is the calculation of the electronic properties of bulk materials. As mentioned above for all four compounds FeVSb, CoTiSb, CoVSn, and NiTiSn, we have adopted the equilibrium lattice constants calculated in Ref. [19], and we present them in Table I together with the band-gap values. All four compounds were found to be nonmagnetic semiconductors, in agreement with previous first-principles calculations [19,28,29,31,32], and in Fig. 2 we present the calculated electronic band structure along the high-symmetry directions in the Brillouin zone. As the band-structure plots reveal, they are indirect band-gap semiconductors since the valence-band maximum (VBM) and the conduction-band minimum (CBM) do not occur at the same

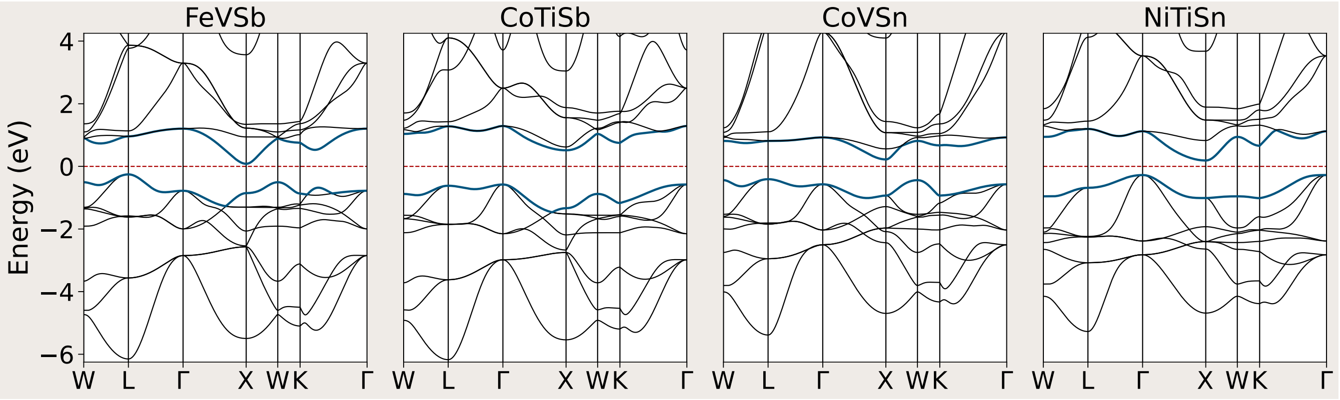

FIG. 2. Band structure of the bulk FeVSb, CoTiSb, CoVSn, and NiTiSn half-Heusler compounds along the high-symmetry lines in the Brillouin zone. With blue, we denote the topmost valence and lowest conduction bands. The zero energy is set as the Fermi level.

high-symmetry points for all compounds. The character of the bands follows the discussion on the minority-spin band structure in half-Heusler compounds [13]. There are exactly nine occupied bands below the Fermi level, and each band accommodates two electrons due to the spin-degeneracy. The lowest band, not shown in Fig. 2, stems from the *s* states of the Sn (Sb) atoms. The lowest shown bands, which are triply degenerate at the Γ point, come from the valence *p* bands of the Sn (Sb) atoms. Afterward, there are two almost flat bands, which are degenerate at the Γ point and stem from the bonding *d* states between the transition-metal atoms. These bonding orbitals are of e_g character. Just below the Fermi level, the bands are triply degenerate at the Γ point and stem from the bonding t_{2g} orbitals between the neighboring transition-metal atoms. These last are separated with a gap from the antibonding *d* states stemming from the hybridization between the *d* states of the transition-metal atoms.

In Table I, we also present the calculated band-gap E_{gap} values, in eV units. The calculated values are, in ascending order, 0.34, 0.47, 0.63, and 1.09 eV for FeVSb, NiTiSb, CoVSn, and CoTiSb, respectively. These values are very close to the ones calculated for the same lattice constants by Ma *et al.* in Ref. [19] (their values were 0.38, 0.44, 0.65, and 1.06, respectively). This shows that the adopted electronic band-structure method for the calculations is not crucial to calculate the properties, and the results depend strongly on the choice of the exchange-correlation functional; in both studies (ours and the study of Ma *et al.*), the PBE parametrization of the GGA functional has been used. Moreover, our result for CoTiSb agrees well with the experimental value of about 1 eV [30].

B. Spin-polarized 2DEG and 2DHG at the interfaces

The study of the bulk systems is followed by a calculation of the interface properties of heterojunctions. First, in Fig. 3, we present the band alignment of all considered heterojunctions. Our four compounds result in six possible heterojunctions, and among them only FeVSb/CoTiSb and CoTiSb/NiTiSn possess type-I band alignment, meaning that the CBM of FeVSb (NiTiSn) is higher than the CBM of CoTiSb, and the VBM of both FeVSb and NiTiSn is lower in energy than the VBM of CoTiSb. All four of the other heterojunctions are of type-II character. Note that the band alignment of the heterojunctions is calculated according to the procedure presented in Ref. [44]. We have simulated the interfaces as discussed in detail in Sec. II, and in Table II we summarize all our results. First, we should note that for each heterostructure, there are two possible terminations at the interface, denoted as Termination-1 when the first compound ends at a pure X layer and Termination-2 when it ends at a mixed YZ layer. As we discussed above in Sec. II, the second compound adopts the in-plane lattice constant of the first compound, and its out-of-plane lattice constant changes accordingly in order to preserve the unit-cell volume as shown by the c/a ratios presented in Table II.

With the exception of the CoTiSb/CoVSn case, in all other studied heterojunctions, the number of valence electrons at the interface is no more 18, but there is either an excess of electrons (Z_t, taking into account the two layers that form the interface, is larger than 18) or a deficit of electrons (Z_t is smaller than 18) and the interface is metallic. In the first case of electron excess, we should have the creation of a 2DEG, while electron deficit can be translated to an excess of holes leading to 2DHG. But as the band structures projected on the

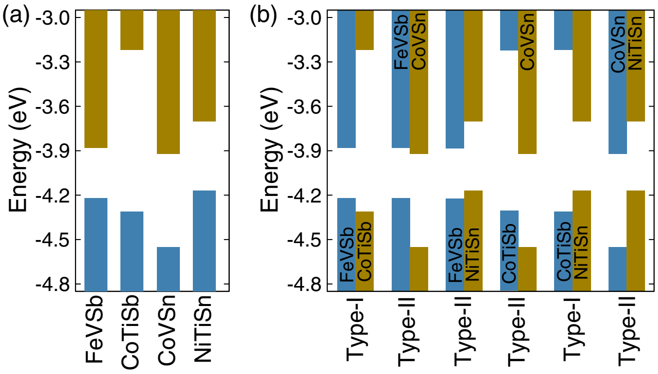

FIG. 3. (a) Calculated position of the valence and conduction bands of bulk Heusler compounds in absolute energy values. (b) Band alignment for the various interfaces under study. Type-I and type-II denote the two possible types of band alignment (see the text for details).

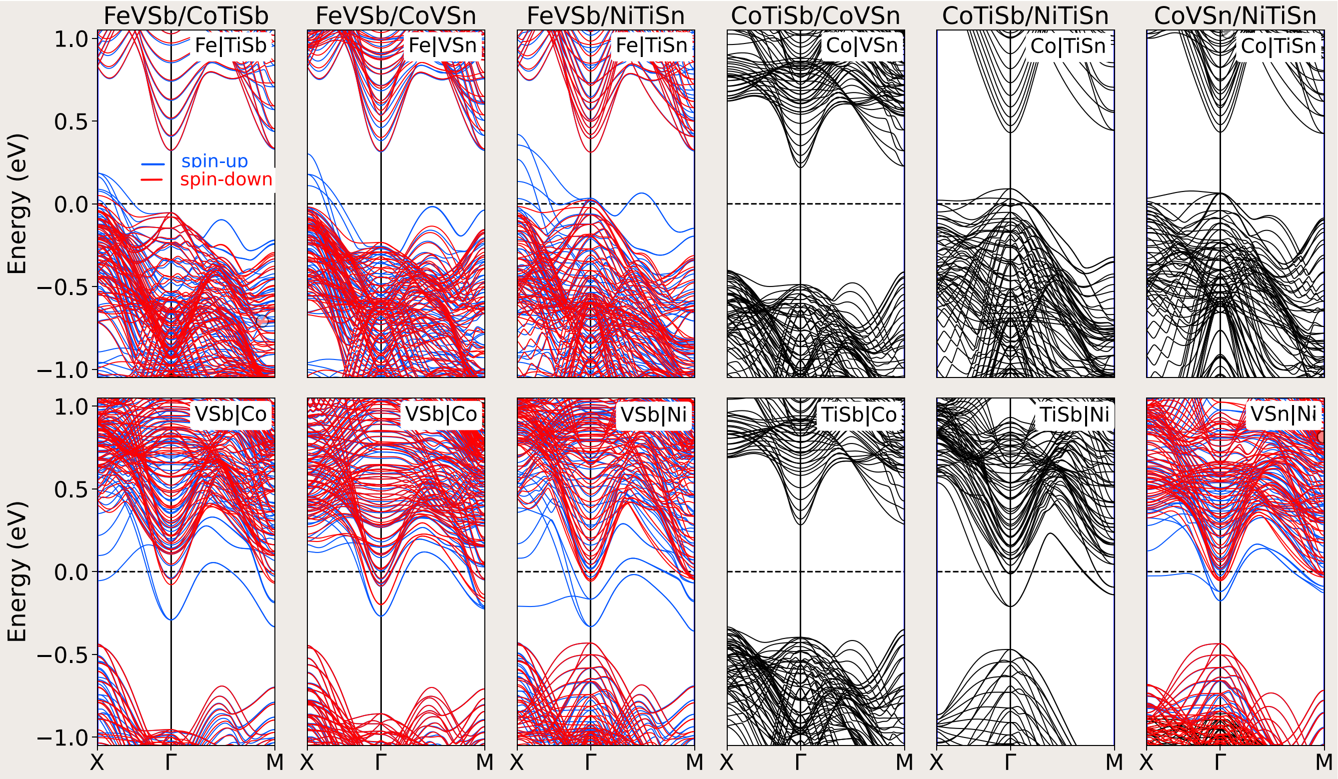

FIG. 4. Band structure for all considered heterojunctions along the X-Γ-M high-symmetry directions of the 2D Brillouin zone.

(001) plane and presented in Fig. 4 reveal, the situation is more complex. In most cases, the metallic interface is also magnetic and the 2DEG (2DHG) is spin-polarized. In Table II we present also the spin magnetic moments of the atoms at the two interface layers as well as the total spin magnetic moment, taking the sum of the spin moments of all interface atoms.

The heterojunctions where FeVSb is one of the two junction materials are the most interesting cases. When Fe is at the interface, there is a deficit of electrons and we have a 2D spin-polarized hole gas (SPHG). In the band structures shown in Fig. 4 this is reflected in the conduction bands, which are crossed by the Fermi level. When the interface layer is VSb and not Fe, there is an excess of electrons leading to 2D spin-polarized electron gas (SPEG) and now the Fermi level crosses the valence bands. Moreover, the Fe and V atoms of FeVSb at the interface and subinterface layers are the ones responsible for the spin-polarized character of the electron (hole) gas. This is depicted clearly in Fig. 5 [panels (a), (b), and (c)], where we present a schematic representation of the layers around the interface for all three heterojunctions containing FeVSb and for both terminations. Arrows show the direction of the atomic spin magnetic moments, and their magnitude is proportional to the values of the spin magnetic moments. In all three heterojunctions presented in the figure, it is easily observed that the magnetic moments reside primarily at the Fe and V atoms at the interface and subinterface layers irrespective of whether we have Fe (Termination-1) or VSb (Termination-2) interface layers.

In the case of Termination-I interfaces, the Fe atoms at the interface layer carry sizable magnetic moments which are antiparallel to the spin magnetic moments of the Ti (V) interface atoms as shown in Table II and schematically in Fig. 5. In the case of Termination-2 interfaces, the Co (Ni) atoms carry very small spin magnetic moments, and it is the V atom at the interface layer of FeVSb which carries again the main portion of the spin magnetic moment. CoVSn/CoTiSb is a particular case due to the presence of Co in both

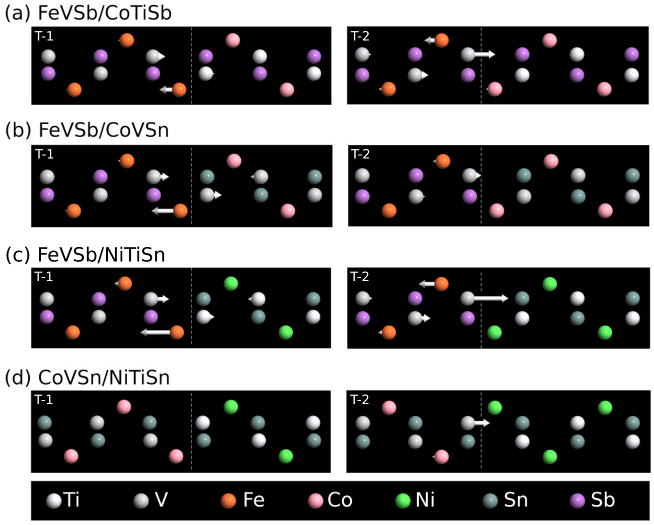

FIG. 5. For both possible interface structures (denoted as T1 and T2) for each system, we show the structure of the interfaces. Arrows denote the direction of the spin magnetic moments of the atoms at the interface, and their magnitude is proportional to the absolute value of the atomic spin magnetic moments presented in Table II.

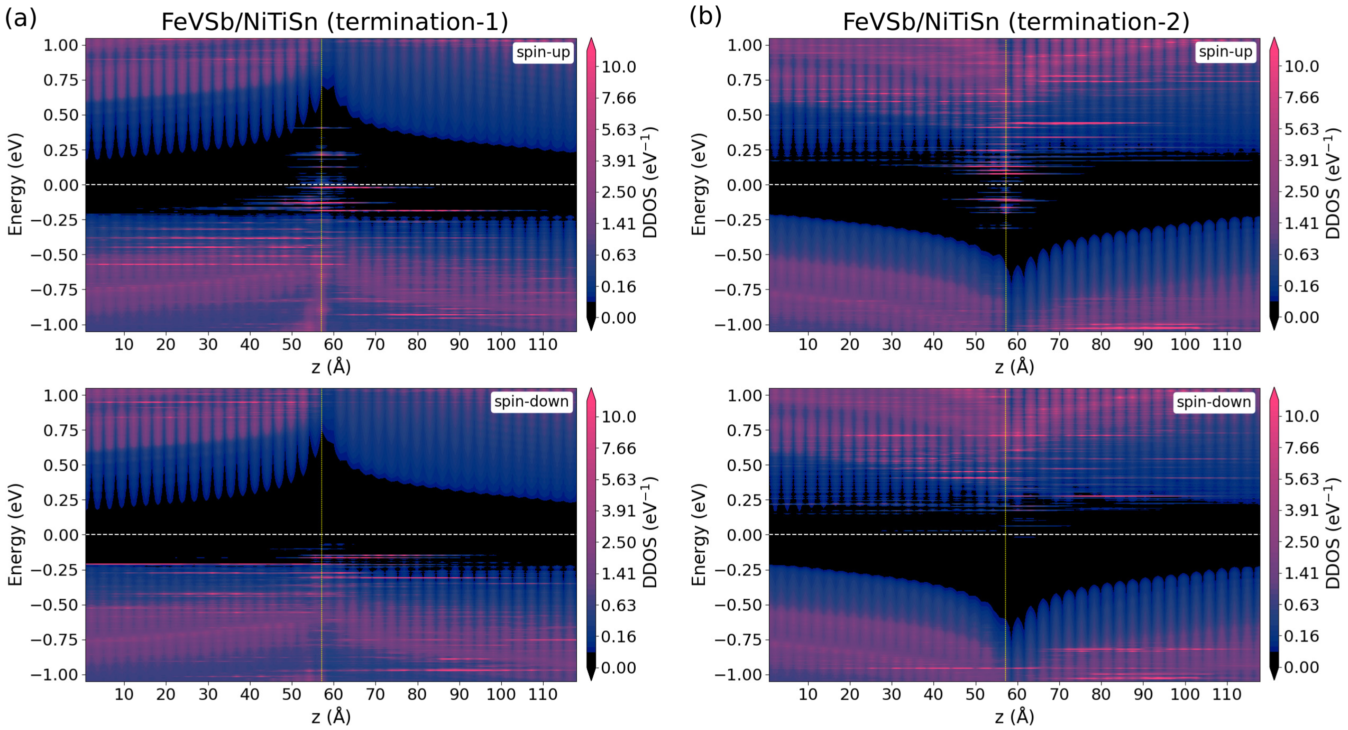

FIG. 6. (a) Projected device density of states (DDOS) for the spin-up (upper panel) and spin-down (lower panel) electrons for the first termination of the FeVSb/NiTiSb junction (the atomic structure for the interface region is given in Fig. 5). The white dashed lines display the Fermi level, while the vertical yellow dashed lines denote the interface. (b) The same as (a) for the second termination.

materials of the heterojunction, and the resulting interface remains semiconducting for both terminations (see Fig. 4). In the case of CoTiSb/NiTiSn interfaces, the interface is metallic but non-spin-polarized and thus we have either a usual 2DEG or 2DHG behavior at the interface as shown in Table II and as can be deduced from Fig. 4. Finally, in the case of the CoVSn/NiTiSn, termination-II is spin-polarized and the 2DEG is also spin-polarized, while termination-I is simply metallic, as deduced also from the band structure in Fig. 4, and there is a usual 2DHG at the interface. The magnetic behavior of the CoVSn/NiTiSn interfaces is also shown in the picture of the atomic spin magnetic moments presented in Fig. 5(d).

To confirm our conclusions, we have also performed device calculations for both possible terminations in the case of the FeVSb/NiTiSn heterostructure. As discussed in Sec. II, device calculations are much more demanding in computer resources than the supercell calculations presented up to now. In this case, we have a 120 Å heterojunction (i.e., the scattering region) with two semi-infinite leads. The obtained spin magnetic moments are similar to the ones obtained using the supercell approach shown in Table II. In Fig. 6 we present for both terminations the spin-up and the spin-down device density of states (DDOS) as a function of the distance. For the spin-up DOS (upper panels) there is a finite DOS around the interface layers which quickly vanishes as we move away from the interface. In the case of the spin-down DOS for both terminations (lower panels) there is a negligible DOS around the Fermi level around the interface region of the device. Thus at the interface, we have a nearly half-metallic magnetic behavior, and as we move away from the interface we get nonmagnetic semiconducting behavior.

The results discussed in the previous paragraph agree well with the conclusions in Ref. [44] regarding the confinement of the electrons and holes at the interface. In Ref. [44] the authors have studied the case of the CoTiSb/NiTiSn heterojunction. At the TiSb-Ni interface, which accommodates a 2DEG, electrons are confined in a region of about 1.5 nm (15 Å) around the interface layer. At the Co-TiSn interface, there is a 2DHG and the holes are confined in a slightly larger region of about 20 Å around the interface. In our case of the FeVSb/NiTiSn heterojunction, as shown in Fig. 6, the change in the DDOS around the interface layer occurs in a region of about 20 Å around the Fermi level in the case of the Fe-TiSn interface and a slightly thicker region in the case of the VSb-Ni interface. Thus the electron and hole gas are confined in a similar region as in Ref. [44].

C. Origin of the spin polarization at the interface

The emergence of interface spin polarization is not straightforward to explain. In most ferromagnetic materials, the Stoner theorem is enough to explain the occurrence of ferromagnetism. Therefore, we will start our discussion based on the Stoner model, even though it was developed for bulk systems.

In materials where the Stoner criterion is fulfilled [$IN(E_F) > 1$, where I is the Stoner parameter and $N(E_F)$ is the non-spin-polarized DOS at the Fermi level], the occurrence of magnetism is favored. To examine whether the Stoner

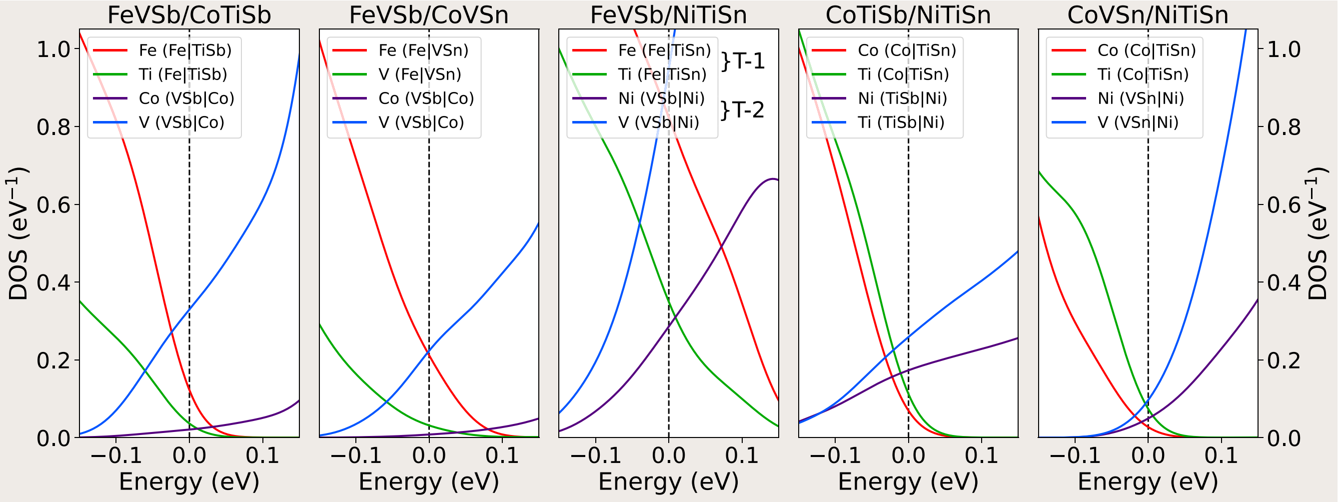

FIG. 7. Atom-resolved nonmagnetic total density of states (DOS) of the transition-metal atoms at the two interface layers around the Fermi level of the heterojunctions.

model can be applied to the interfaces, one should first estimate the value of I and $N(E_F)$. For the latter in Fig. 7 we have plotted the non-spin-polarized DOS around the Fermi level for the atoms at the interface of heterojunctions except the CoTiSb/CoVSn one, which is a nonmagnetic semiconductor. One can easily see that the FeVSb/NiTiSn heterojunction for both terminations presents a significantly larger DOS at the Fermi level than all other cases which approach the value of 1 eV^{-1}.

To estimate the value of the Stoner parameter I, we can use the relationship $I = \frac{U+6J}{5}$ proposed by Stollhoff *et al.* [70] for bulk materials, where U is and J are the Hubbard on-site Coulomb repulsion and the exchange parameters, respectively. These parameters are hard to extract experimentally and their *ab initio* calculation is very demanding. In Ref. [71], their values have been calculated for several Heusler materials including also some half-Heusler compounds using the constrained random-phase approximation. For the transition-metal atoms of half-Heusler compounds, the U parameters calculated in Ref. [71] vary between 3 and 4 eV and the J parameter is around 0.7 eV. We expect that since these values are for bulk systems, in the case of 2D systems like the ones studied here, the U values will be slightly larger due to reduced screening stemming from the out-of-plane atoms in the heterojunctions. Thus, using the U and J values from Ref. [71], the relation mentioned above gives for the I parameter a value of 1–1.4 eV. According to this, we should expect that only the two terminations of the FeVSb/NiTiSn heterojunction should present a spin-polarized electronic band structure at the interface. But the Stoner model for itinerant magnetism is a mean-field treatment missing the effect of strong electronic correlations. The latter can induce also magnetic order [72] as it seems to be the case for all the other interfaces which present a low DOS at the Fermi level as shown in Fig. 7 and do not fulfill the Stoner criterion.

D. Modified Slater-Pauling rules for interfaces

Slater-Pauling rules in the case of Heusler compounds were initially formulated in the case of half-metallic Heuslers crystallizing in the $C1_b$ lattice as the one adopted by the present compounds [13]. These rules connect the half-metallicity and the magnetic properties in the case of Heusler compounds. It was shown in Ref. [13] that the total spin magnetic moment in the unit cell M_t in μ_B units is just the total number of valence electrons in the unit cell, Z_t minus 18 for half-metals ($M_t = Z_t - 18$). This rule expresses the fact that in the spin-down band structure, where the energy gap exists, there are exactly 9 completely occupied bands. When Z_t equals 18, the total spin magnetic moment is zero. Since in the Heusler compounds crystallizing in the $C1_b$ lattice, conventional antiferromagnetism cannot occur due to symmetry reasons, the 18 valence electron Heusler compounds have to be semiconductors or completely compensated ferrimagnetic half-metals. This prediction is in agreement with the behavior of FeVSb, CoVSn, CoTiSb, and NiTiSn compounds.

The question that rises is whether it is possible to formulate the Slater-Pauling rule in a way to connect the magnetic properties of the studied heterojunctions with the total number of valence electrons at the interface. To answer this question, one should consider the (001) planes of the lattice shown in Fig. 1, and we will use FeVSb as the example. The (001) planes are made up either of pure Fe or mixed V-Sb atoms. The FeVSb unit cell has in total 18 valence electrons; Fe contributes 8 valence electrons, and the V-Sb atoms 10. In a representation like the one shown in Fig. 8, each Fe plane contributes 4 electrons to the bonds with the VSb plane on its right and another 4 electrons to build up bonds with the VSb plane on its left. Following the same reasoning, each VSb plane contributes 5 electrons to each one of its two sides. Thus in total 9 electrons contribute to the bonding between the atoms in two consecutive layers. The same reasoning stands also for NiTiSn, but now Ni planes contribute 5 electrons to the bonds with each one of the neighboring TiSn layers, and each TiSn layer contributes 4 electrons to the corresponding bonds. At the VSb-Ni or TiSn-Fe interfaces shown in Fig. 8 we have now 10 or 8 electrons, respectively, contributing to the bonding between the atoms at the interface layers. The total number of these electrons is $Z_t/2$, where Z_t refers to

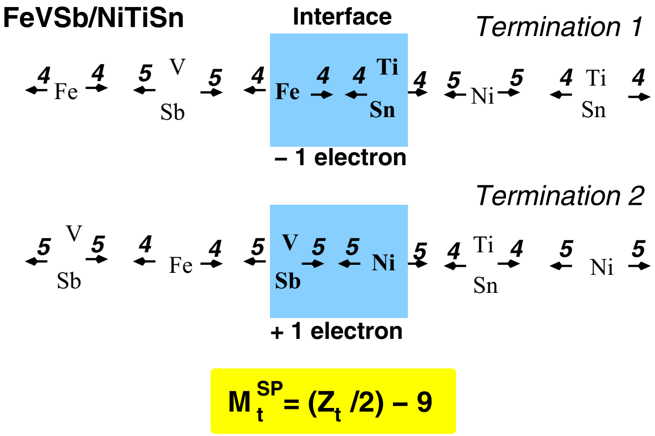

FIG. 8. Schematic representation of the bonding in the two possible FeVSb-NiTiSn interfaces. For the half-metallic materials from both sides of the interface, the bonds between the atoms at two consecutive layers are built up from nine valence electrons. The numbers on top of the arrows show the valence electrons contributed by each layer (e.g., VSb has ten valence electrons which are split for the bonds at the two sides of the VSb layer). At the interface, the electrons contributing at the bonding are $\frac{Z_t}{2}$ (see Table II for the definition). Thus the excess or shortage of valence electrons at the interface with respect to the nine within the rest of the material is $\frac{Z_t}{2} - 9$. To achieve half-metallicity, these extra (less) valence electrons should occupy (vacate) spin-up states leading to a modified Slater-Pauling rule for the total spin magnetic moment at the interface: $M_t^{SP} = \frac{Z_t}{2} - 9$, where M_t^{SP} is in μ_B.

the compound built up from the atoms at the interface (e.g., NiVSb or FeTiSn in our case) and thus the difference with the nine electrons of the perfect semiconducting interface is $Z_t/2 - 9$. This means that at the VSb-Ni interface there is a surplus of one electron, while at the TiSn-Fe interface there is a shortage of one electron. Thus the prerequisite for half-metallicity at the interfaces is that the total spin magnetic moment at the interface follows a modified Slater-Pauling rule of the $M_t = Z_t/2 - 9$ form.

To verify the validity of the proposed modified Slater-Pauling rule, in Table II we present the calculated total spin magnetic moment for all interfaces taking into account either the two interface layers only or the whole cell used for the calculations with respect to the ones predicted by the Slater-Pauling rule. For the discussion, we take into account the electronic character of the interface as presented in Fig. 4 where the (001) projected band structures for all interfaces are presented. The calculated total spin magnetic moments are very close to the ones predicted by the Slater-Pauling rule for half-metallic behavior (deviation less than $0.05\mu_B$) in the case in which FeVSb is part of the heterojunction and Fe is at the interface as well as for the VSn-Ni interface. If we examine the band structures presented in Fig. 4, the Fe-VSn interface is a perfect half-metal. But even in the case of the Fe-VSn interface, the calculated total spin magnetic moment in the simulation cell is $-0.46\mu_B$, slightly deviating from the ideal $-0.5\mu_B$ predicted by the Slater-Pauling rule. This is due to the numerical accuracy of the Mulliken population method in the QUANTUMATK code, which we have employed when calculating the atomic spin magnetic moments. In the case of the Fe-TiSb interface, the Fermi level slightly crosses the spin-down valence band, while in the case of VSb-Co and VSn-Ni interfaces, the Fermi level slightly crosses the spin-down conduction band. Both types of interfaces between the CoTiSb and CoVSn compounds are semiconducting, in agreement with the Slater-Pauling rule. For the rest of the interfaces, the Slater-Pauling rule is not obeyed and the electronic character of the interfaces is no longer half-metallic. The above discussion is reflected on the calculated spin-polarization SP presented in the last column of Table II. It is defined as $\frac{n^{\uparrow}-n^{\downarrow}}{n^{\uparrow}+n^{\downarrow}}$, where $n^{\uparrow(\downarrow)}$ is the density of states at the Fermi level for the spin-up (-down) electrons. A value of 100% means a half-metallic interface, while values larger than 70% mean that more than 85% of the electrons at the Fermi level are of spin-up character.

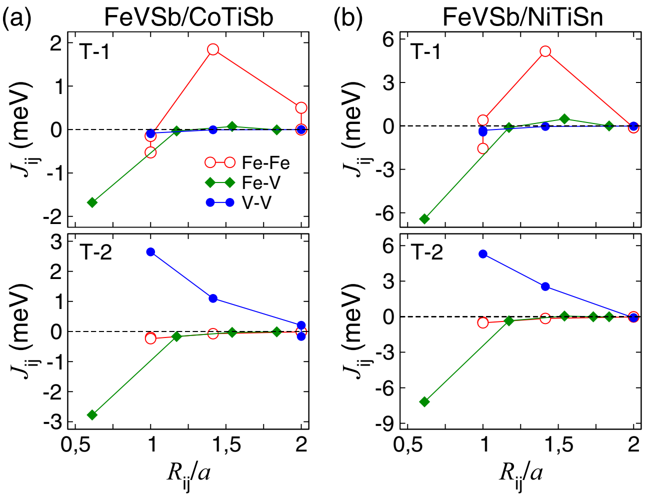

FIG. 9. (a) Calculated intra-sublattice (Fe-Fe and V-V) and inter-sublattice (Fe-V) Heisenberg exchange parameters as a function of distance for the interface and subinterface layers of the FeVSb/CoTiSb heterojunction for both possible T-1 and T-2 interface terminations. (b) The same as (a) for the FeVSb/NiTiSn heterojunction. For the definition of T-1 and T-2, see Figs. 1 and 5.

E. Exchange interactions and Curie temperature

In the last part of our study, we compute the Heisenberg exchange parameters as discussed in detail in Sec. II. We have chosen the FeVSb/CoTiSb and FeVSb/NiTiSn heterojunctions since in their case atoms at the interface carry sizable spin magnetic moments for both terminations. We present our results in Fig. 9. The upper panels refer to Termination-1, where the interface is Fe-TiSb (TiSn), and the lower panels refer to Termination-2, where the interface layers are VSb-Co(Ni). We restrict ourselves to FeVSb only, since only the Fe and V atoms at the interface present significant spin magnetic moments, and we present the exchange constants as a function of the distance for the Fe and V atoms at the interface and subinterface layers. The first striking characteristic feature in all cases is the strong negative exchange parameters between the nearest-neighbor Fe-V atoms. This is reflected in the antiparallel Fe-V spin magnetic moments, which stabilize the magnetic order at the interface. In the case of Termination-1, the V atoms are at the subinterface

TABLE III. Calculated magnetic anisotropy energy (MAE) provided per supercell simulation cell and the interface Curie temperature T_C for the FeVSb/CoTiSb (NiTiSn) heterojunctions for both possible interface terminations. In square brackets, we include the MAE values in the case of the FeVSb/CoTiSb heterojunction assuming that CoTiSb keeps its bulk lattice constant and relaxing FeVSb lattice.

Semi-Heusler heterojunction	Interface termination	MAE = $(E_{\|\|} - E_{\perp})$ (μeV/cell)	T_{C} (K)
FeVSb/CoTiSb	Fe|TiSb	−121.3 [−209.8]	78
	VSb|Co	−76.6 [−104.9]	101
FeVSb/NiTiSn	Fe|TiSn	8.5	187
	VSb|Ni	−24.9	248

layer, the V has negligible spin magnetic moments, and the V-V exchange constants are vanishing. In the case of Termination-2, the V atoms are at the interface layer and they carry a sizable spin magnetic moment, as shown in Table II (see also Fig. 5), and the V-V exchange interactions are all positive, favoring the ferromagnetic alignment of the V spin magnetic moments. For Termination-2, the interactions between the Fe atoms located at the subinterface layer are negligible as expected. Interestingly in the Termination-1 cases, the Fe-Fe exchange parameters are sizable for both FeVSb/CoTiSb and FeVSb/NiTiSn heterojunctions favoring the ferromagnetic alignment of the Fe spin magnetic moments at the interface layers. We used the calculated exchange parameters to estimate the Curie temperature T_{C} within the mean-field approximation (MFA), and we present our results in Table III. In our calculation, we took into account exchange interactions between atoms at six to seven layers around the interface accounting for the interactions between atoms at all layers having a spin magnetic moment larger than $0.1\mu_{\mathrm{B}}$. The obtained values range from about 78 K to about 248 K, being larger for the FeVSb/NiTiSn heterostructure and for Termination-2 with respect to Termination-1. These values are relatively small when compared to room temperature. Unfortunately, no experimental data on the Curie temperatures exist in the literature for comparison to establish the accuracy of our calculations. Such a comparison would be necessary since (i) MFA ignores spin-fluctuations, which are important, especially for low-dimensional magnets tending to overestimate T_{C}, and (ii) for systems with small spin magnetic moments (less than 1 μ_{B}), the exchange parameters J_{ij} are underestimated when using the linear-response theory (as is the case here) and thus the T_{C} is also underestimated [73]. These two phenomena induce competing errors, and this explains the behavior of calculated T_{C} in bulk half-ferromagnetic Heusler compounds; in the case of NiMnSn where the Mn spin magnetic moment is very large, the MFA overestimates the T_{C} by about 400 K, while in Co_2CrAl and Co_2MnSi full-Heusler compounds due to the much smaller spin magnetic moments, MFA is much more accurate and underestimates T_{C} by about 50–100 K only [74]. In the case of the studied interfaces due to the small spin magnetic moments at the interface, we expect that the errors induced by the two competing phenomena will almost cancel each other out, and the agreement with the experiment will be even better than in full-Heusler compounds.

Finally, in Table III we also present the calculated values of the magnetic anisotropy energy (MAE) for FeVSb in μeV per simulation supercell. All systems possess small values of MAE of the order of 0.1 meV. As shown in Ref. [75], even very small values of the MAE lead to finite values of the Curie temperature. In all cases, the easy magnetization axis is parallel to the interface with the exception of Termination-1 in the FeVSn/NiTiSn system, where the easy magnetization axis is perpendicular to the interface but the MAE is almost vanishing. The magnetization easy axis is determined from the interplay between the magnetoelastic, magnetosurface, and shape anisotropies. The first two in the case of Fe layers at the interface usually favor a perpendicular magnetization axis, while shape anisotropy, which is the dominating contribution in most cases, favors an in-plane magnetization axis [76]. As discussed above, when we considered our supercells, FeVSb adopted in all studied cases a cubic lattice, and we relaxed the cell only of the other material in the heterojunction. This explains the very small calculated MAE values. If the opposite procedure takes place and now FeVSb is grown on top of the other material (e.g., CoTiSb), the latter will adopt a cubic lattice, and FeVSb will adopt the same in-plane lattice constant. This will lead to a tetragonal structure for the FeVSb material and much larger MAE values [12] since materials tend to keep their unit-cell volume almost constant and change their lattice parameters accordingly. We performed such MAE calculations assuming the cubic lattice for CoTiSb and relaxing the structure for FeVSb. We include our calculated results in Table III. CoTiSb has a larger lattice constant in its bulk phase with respect to FeVSb (see Table I). Thus FeVSb is considerably strained, and with respect to the heterojunction where it keeps its cubic lattice, MAE is considerably increased. The increase of the absolute value of the MAE is 37% in the case of the second termination, and almost double, 73%, in the case of the first termination.

IV. SUMMARY AND CONCLUSIONS

Half-Heusler compounds, which have 18 valence electrons per unit cell, like FeVSb, CoTiSb, CoVSn, and NiTiSn, are well-known for their nonmagnetic semiconducting properties. In the present study, we employed first-principles electronic band-structure calculations and examined the properties of the interfaces of the heterojunctions based on these four half-Heusler compounds. First, we confirmed the nonmagnetic semiconducting character of these compounds in their bulk form. Then we used a supercell approach to study the heterojunction interfaces considering the [001] axis as the growth direction. Our results suggest the formation of a two-dimensional electron (2DEG) or hole (2DHG) gas at the interfaces. Several of these interfaces exhibit not only metallic behavior but also magnetic behavior in some cases. These unique characteristics make these structures potentially useful for spintronic applications. To further understand the magnetic properties of the interfaces of heterojunctions, we developed a modified Slater-Pauling rule that is similar to the corresponding rule for the bulk half-metallic half-Heusler compounds. This rule connects the altered number of valence electrons at the interface to the total spin magnetic moment at the interface and is a prerequisite for half-metallicity to occur. We also calculated other properties of interest, such as exchange parameters, Curie temperature, and magnetic anisotropy energies.

Overall, our study adds to the growing body of knowledge on the properties of half-Heusler heterojunction interfaces and their potential for use in spintronic and magnetoelectronic devices. We hope that our findings, combined with recent experimental evidence for the presence of 2DEG at CoTiSb/NiTiSn heterojunctions [50], will increase interest in these materials and their potential applications. We expect our study to motivate future efforts and studies toward the experimental realization of devices using the proposed heterojunctions.

ACKNOWLEDGMENTS

This work was supported by SFB CRC/TRR 227 of Deutsche Forschungsgemeinschaft (DFG) and by the European Union (EFRE) via Grant No. ZS/2016/06/79307. B.S. acknowledges financial support from Swedish Research Council (Grant No. 2022-04309). The computations were enabled in project SNIC 2022/3-30 by resources provided by the Swedish National Infrastructure for Computing (SNIC) at NSC, PDC, and HPC2N partially funded by the Swedish Research Council (Grant No. 2018-05973). B.S. acknowledges allocation of supercomputing hours by PRACE DECI-17 project "Q2Dtopomat" in the Eagle supercomputer in Poland and EuroHPC resources in the Karolina supercomputer in Czech Republic.

[1] F. Heusler, Kristallstruktur und ferromagnetismus der Mangan-Aluminium-kupferlegierungen, Verh. Dtsch. Phys. Ges. **12**, 219 (1903).

[2] F. Heusler and E. Take, The nature of the Heusler alloys, Phys. Z. **13**, 897 (1912).

[3] T. Graf, C. Felser, and S. S. P. Parkin, Simple rules for the understanding of Heusler compounds, Prog. Solid State Chem. **39**, 1 (2011).

[4] S. Tavares, K. Yang, and M. A. Meyers, Heusler alloys: Past, properties, new alloys, and prospects, Prog. Mater. Sci. **132**, 101017 (2023).

[5] S. Chatterjee, S. Chatterjee, S. Giri, and S. Majumdar, Transport properties of Heusler compounds and alloys, J. Phys.: Condens. Matter **34**, 013001 (2022).

[6] M. I. Katsnelson, V. Y. Irkhin, L. Chioncel, A. I. Lichtenstein, and R. A. de Groot, Half-metallic ferromagnets: From band structure to many-body effects, Rev. Mod. Phys. **80**, 315 (2008).

[7] I. Galanakis, K. Özdoğan, and E. Şaşıoğlu, Spin-filter and spin-gapless semiconductors: The case of Heusler compounds, AIP Adv. **6**, 055606 (2016).

[8] E. Şaşıoğlu, S. Blügel, and I. Mertig, Proposal for reconfigurable magnetic tunnel diode and transistor, ACS Appl. Electron. Mater. **1**, 1552 (2019).

[9] E. Şaşıoğlu, T. Aull, D. Kutschabsky, S. Blügel, and I. Mertig, Half-Metal–Spin-Gapless-Semiconductor Junctions as a Route to the Ideal Diode, Phys. Rev. Appl. **14**, 014082 (2020).

[10] J. K. Kawasaki, Heusler interfaces–Opportunities beyond spintronics?, APL Mater. **7**, 080907 (2019).

[11] T. Aull, E. Şaşıoğlu, I. V. Maznichenko, S. Ostanin, A. Ernst, I. Mertig, and I. Galanakis, *Ab initio* design of quaternary Heusler compounds for reconfigurable magnetic tunnel diodes and transistors, Phys. Rev. Mater. **3**, 124415 (2019).

[12] T. Aull, E. Şaşıoğlu, and I. Mertig, First principles design of Ohmic spin diodes based on quaternary Heusler compounds, Appl. Phys. Lett. **118**, 052405 (2021).

[13] I. Galanakis, P. H. Dederichs, and N. Papanikolaou, Origin and properties of the gap in the half-ferromagnetic Heusler alloys, Phys. Rev. B **66**, 134428 (2002).

[14] I. Galanakis, P. H. Dederichs, and N. Papanikolaou, Slater-Pauling behavior and origin of the half-metallicity of the full-Heusler alloys, Phys. Rev. B **66**, 174429 (2002).

[15] I. Galanakis, Appearance of half-metallicity in the quaternary Heusler alloys, J. Phys.: Condens. Matter **16**, 3089 (2004).

[16] S. Skaftouros, K. Ozdogan, E. Şaşıoğlu, and I. Galanakis, Generalized Slater-Pauling rule for the inverse Heusler compounds, Phys. Rev. B **87**, 024420 (2013).

[17] K. Ozdogan, E. Şaşıoğlu, and I. Galanakis, Slater-Pauling behavior in LiMgPdSn-type multifunctional quaternary Heusler materials: Half-metallicity, spin-gapless and magnetic semiconductors, J. Appl. Phys. **113**, 193903 (2013).

[18] S. Nepal, R. Dhakal, I. Galanakis, S. M. Winter, R. P. Adhikari, and G. C. Kaphle, *Ab initio* study of stable $3d$, $4d$, and $5d$ transition-metal-based quaternary Heusler compounds, Phys. Rev. Mater. **6**, 114407 (2022).

[19] J. Ma, V. I. Hegde, K. Munira, Y. Xie, S. Keshavarz, D. T. Mildebrath, C. Wolverton, A. W. Ghosh, and W. H. Butler, Computational investigation of half-Heusler compounds for spintronics applications, Phys. Rev. B **95**, 024411 (2017).

[20] M. Gilleßen and R. Dronskowski, A combinatorial study of full Heusler alloys by first-principles computational methods, J. Comput. Chem. **30**, 1290 (2009).

[21] M. Gilleßen and R. Dronskowski, A combinatorial study of inverse Heusler alloys by first-principles computational methods, J. Comput. Chem. **31**, 612 (2010).

[22] S. V. Faleev, Y. Ferrante, J. Jeong, M. G. Samant, B. Jones, and S. S. P. Parkin, Unified explanation of chemical ordering, the Slater-Pauling rule, and half-metallicity in full Heusler compounds, Phys. Rev. B **95**, 045140 (2017).

[23] S. V. Faleev, Y. Ferrante, J. Jeong, M. G. Samant, B. Jones, and S. S. P. Parkin, Origin of the Tetragonal Ground State of Heusler Compounds, Phys. Rev. Appl. **7**, 034022 (2017).

[24] S. V. Faleev, Y. Ferrante, J. Jeong, M. G. Samant, B. Jones, and S. S. P. Parkin, Heusler compounds with perpendicular magnetic anisotropy and large tunneling magnetoresistance, Phys. Rev. Mater. **1**, 024402 (2017).

[25] Q. Gao, I. Opahle, and H. Zhang, High-throughput screening for spin-gapless semiconductors in quaternary Heusler compounds, Phys. Rev. Mater. **3**, 024410 (2019).

[26] Y. Han, Z. Chen, M. Kuang, Z. Liu, X. Wang, and X. Wang, 171 Scandium-based full Heusler compounds: A comprehensive study of competition between XA and $L2_1$ atomic ordering, Res. Phys. **12**, 435 (2019).

[27] D. Jung, H.-J. Koo, and M.-H. Whangbo, Study of the 18-electron band gap and ferromagnetism in semi-Heusler compounds by non-spin-polarized electronic band structure calculations, J. Mol. Struct.:THEOCHEM **527**, 113 (2000).

[28] J. Pierre, R. V. Skolozdra, Y. K. Gorelenko, and M. Kouacou, From nonmagnetic semiconductor to itinerant ferromagnet in the TiNiSn-TiCoSn series, J. Magn. Magn. Mater. **134**, 95 (1994).

[29] J. Tobola, J. Pierre, S. Kaprzyk, R. Skolozdra, and M. Kouacou, Crossover from semiconductor to magnetic metal in semi-Heusler phases as a function of valence electron concentration, J. Phys.: Condens. Matter **10**, 1013 (1998).

[30] S. Ouardi, G. H. Fecher, C. Felser, M. Schwall, S. S. Naghavi, A. Gloskovskii, B. Balke, J. Hamrle, K. Postava, J. Pištora, S. Ueda, and K. Kobayashi, Electronic structure and optical, mechanical, and transport properties of the pure, electron-doped, and hole-doped Heusler compound CoTiSb, Phys. Rev. B **86**, 045116 (2012).

[31] C. Lue, Y. Oner, D. Naugle, and J. Ross, Magnetism of new semi-Heusler compounds FeVSn and CoVSn, IEEE Trans. Magn. **37**, 2138 (2001).

[32] M. Mokhtari, F. Dahmane, G. Benabdellah, L. Zekri, S. Benalia, and N. Zekri, Theoretical study of the structural stability, electronic and magnetic properties of XVSb (X = Fe, Co, and Ni) half-Heusler compounds, Condens. Matter Phys. **21**, 43705 (2018).

[33] E. H. Shourov, R. Jacobs, W. A. Behn, Z. J. Krebs, C. Zhang, P. J. Strohbeen, D. Du, P. M. Voyles, V. W. Brar, D. D. Morgan, and J. K. Kawasaki, Semi-adsorption-controlled growth window for half-Heusler FeVSb epitaxial films, Phys. Rev. Mater. **4**, 073401 (2020).

[34] K. Kroth, B. Balke, G. H. Fecher, V. Ksenofontov, C. Felser, and H.-J. Lin, Diluted magnetic semiconductors with high curie temperature based on C1(b) compounds: $CoTi_{1-x}Fe_xSb$, Appl. Phys. Lett. **89**, 202509 (2006).

[35] N. Naghibolashrafi, V. I. Hegde, K. C. Shambhu, S. Keshavarz, S. S. Naghavi, J. Ma, A. Gupta, P. LeClair, W. H. Butler, C. Wolverton, K. Munira, D. Mazumdar, and A. W. Ghosh, Structural and magnetic analyses of the $Fe_xCo_{1-x}TiSb$ alloy system: $Fe_{0.5}Co_{0.5}TiSb$ as a prototypical half-Heusler compound, J. Alloys Compd. **822**, 153408 (2020).

[36] B. Nanda and I. Dasgupta, Electronic structure and magnetism in doped semiconducting half-Heusler compounds, J. Phys.: Condens. Matter **17**, 5037 (2005).

[37] B. Sanyal, O. Eriksson, K. G. Suresh, I. Dasgupta, A. K. Nigam, and P. Nordblad, Ferromagnetism in Mn doped half-heusler NiTiSn: Theory and experiment, Appl. Phys. Lett. **89**, 212502 (2006).

[38] N. Y. Sun, Y. Q. Zhang, W. R. Che, J. Qin, and R. Shan, Structural, magnetic, and transport properties of Fe-doped CoTiSb epitaxial thin films, J. Appl. Phys. **118**, 173905 (2015).

[39] N. Tareuchi, K. Gosho, M. Hiroi, and M. Kawakami, The effect of V substitution on the properties of CoTiSb, Phys. B: Condens. Matter **359-361**, 1183 (2005).

[40] J. Tobola and J. Pierre, Electronic phase diagram of the XTZ (X = Fe, Co, Ni; T = Ti, V, Zr, Nb, Mn; Z = Sn, Sb) semi-Heusler compounds, J. Alloys Compd. **296**, 243 (2000).

[41] J. Tobola, S. Kaprzyk, and P. Pecheur, Theoretical search for magnetic half-Heusler semiconductors, Phys. Status Solidi B **236**, 531 (2003).

[42] B. Balke, G. H. Fecher, A. Gloskovskii, J. Barth, K. Kroth, C. Felser, R. Robert, and A. Weidenkaff, Doped semiconductors as half-metallic materials: Experiments and first-principles calculations of $CoTi_{1-x}m_xSb$ (M = Sc, V, Cr, Mn, Fe), Phys. Rev. B **77**, 045209 (2008).

[43] Z. Zhu, Y. Cheng, and U. Schwingenschloegl, Vacancy induced half-metallicity in half-Heusler semiconductors, Phys. Rev. B **84**, 113201 (2011).

[44] A. Sharan, Z. Gui, and A. Janotti, Formation of two-dimensional electron and hole gases at the interface of half-Heusler semiconductors, Phys. Rev. Mater. **3**, 061602 (2019).

[45] J. Betancourt, T. R. Paudel, E. Y. Tsymbal, and J. P. Velev, Spin-polarized two-dimensional electron gas at $GdTiO_3/SrTiO_3$ interfaces: Insight from first-principles calculations, Phys. Rev. B **96**, 045113 (2017).

[46] A. Ohtomo, D. A. Muller, J. L. Grazul, and H. Hwang, Artificial charge-modulation in atomic-scale perovskite titanate superlattices, Nature (London) **419**, 378 (2002).

[47] A. Ohtomo and H. Hwang, A high-mobility electron gas at the $LaAlO_3/SrTiO_3$ heterointerface, Nature (London) **427**, 423 (2004).

[48] N. T. Linh, The two-dimensional electron gas and its technical applications, in *Festkörperprobleme 23: Plenary Lectures of the Divisions "Semiconductor Physics" "Metal Physics" "Low Temperature Physics" "Thermodynamics and Statistical Physics" "Thin Films" "Surface Physics" "Surface Physics" "Magnetism" of the German Physical Society (DPG) Freudenstadt, March 21–25, 1983*, edited by P. Grosse (Springer, Berlin, 1983), pp. 227–257.

[49] S. Keshavarz, I. Di Marco, D. Thonig, L. Chioncel, O. Eriksson, and Y. O. Kvashnin, Magnetic two-dimensional electron liquid at the surface of Heusler semiconductors, Phys. Rev. Mater. **4**, 021401(R) (2020).

[50] S. D. Harrington, Semiconducting Half-Heusler Based Compounds and Heterostructures Grown by Molecular Beam Epitaxy, Ph.D. thesis, University of California Santa Barbara (2018).

[51] S. Jenkins, L. Rozsa, U. Atxitia, R. F. L. Evans, K. S. Novoselov, and E. J. G. Santos, Breaking through the Mermin-Wagner limit in 2D van der Waals magnets, Nat. Commun. **13**, 6917 (2022).

[52] G. Kresse and J. Hafner, Norm-conserving and ultrasoft pseudopotentials for first-row and transition elements, J. Phys.: Condens. Matter **6**, 8245 (1994).

[53] G. Kresse and D. Joubert, From ultrasoft pseudopotentials to the Projector Augmented-Wave method, Phys. Rev. B **59**, 1758 (1999).

[54] J. P. Perdew, K. Burke, and M. Ernzerhof, Generalized Gradient Approximation Made Simple, Phys. Rev. Lett. **77**, 3865 (1996).

[55] S. Smidstrup, D. Stradi, J. Wellendorff, P. A. Khomyakov, U. G. Vej-Hansen, M.-E. Lee, T. Ghosh, E. Jónsson, H. Jónsson, and K. Stokbro, First-principles Green's-function method for surface calculations: A pseudopotential localized basis set approach, Phys. Rev. B **96**, 195309 (2017).

[56] S. Smidstrup, T. Markussen, P. Vancraeyveld, J. Wellendorff, J. Schneider, T. Gunst, B. Verstichel, D. Stradi, P. A. Khomyakov, U. G. Vej-Hansen, M.-E. Lee, S. T. Chill, F. Rasmussen, G. Penazzi, F. Corsetti, A. Ojanpera, K. Jensen, M. L. N. Palsgaard, U. Martinez, A. Blom, M. Brandbyge, and K. Stokbro, QuantumATK: An integrated platform of electronic and atomic-scale modelling tools, J. Phys.: Condens. Matter **32**, 015901 (2020).

[57] M. J. van Setten, M. Giantomassi, E. Bousquet, M. J. Verstraete, D. R. Hamann, X. Gonze, and G. M. Rignanese, The PSEUDODOJO: Training and grading a 85 element optimized norm-conserving pseudopotential table, Comput. Phys. Commun. **226**, 39 (2018).

[58] H. J. Monkhorst and J. D. Pack, Special points for Brillouin-zone integrations, Phys. Rev. B **13**, 5188 (1976).

[59] T. Block, M. J. Carey, B. A. Gurney, and O. Jepsen, Band-structure calculations of the half-metallic ferromagnetism and structural stability of full- and half-Heusler phases, Phys. Rev. B **70**, 205114 (2004).

[60] A. I. Liechtenstein, M. I. Katsnelson, V. P. Antropov, and V. A. Gubanov, Local spin density functional approach to the theory of exchange interactions in ferromagnetic metals and alloys, J. Magn. Magn. Mater. **67**, 65 (1987).

[61] J. M. Wills, M. Alouani, P. Andersson, A. Delin, O. Eriksson, and O. Grechnyev, *Full-Potential Electronic Structure Method: Energy and Force Calculations With Density Functional and Dynamical Mean Field Theory*, Springer Series in Solid-State Sciences Vol. 167 (Springer, Berlin, Heidelberg, 2010).

[62] P. W. Anderson, Theory of magnetic exchange interactions: Exchange in insulators and semiconductors, in *Solid State Physics*, edited by F. Seitz and D. Turnbull (Academic Press, New York, 1987), Vol. 14, pp. 99–214.

[63] E. Şaşıoğlu, L. M. Sandratskii, and P. Bruno, First-principles calculation of the intersublattice exchange interactions and curie temperatures of the full heusler alloys $\mathrm{Ni_2MnX}$ (X = Ga, In, Sn, Sb), Phys. Rev. B **70**, 024427 (2004).

[64] S. Yamada, S. Kobayashi, F. Kuroda, K. Kudo, S. Abo, T. Fukushima, T. Oguchi, and K. Hamaya, Magnetic and transport properties of equiatomic quaternary heusler CoFeVSi epitaxial films, Phys. Rev. Mater. **2**, 124403 (2018).

[65] A. J. Garza and S. G. E., Predicting band gaps with hybrid density functionals, J. Phys. Chem. Lett. **7**, 4165 (2016).

[66] J. Heyd, G. E. Scuseria, and M. Ernzerhof, Hybrid functionals based on a screened Coulomb potential, J. Chem. Phys. **118**, 8207 (2003).

[67] J. Heyd, G. E. Scuseria, and M. Ernzerhof, Erratum: Hybrid functionals based on a screened Coulomb potential [J. Chem. Phys. **118**, 8207 (2003)], J. Chem. Phys. **124**, 219906 (2006).

[68] M. Tas, E. Şaşıoğlu, I. Galanakis, C. Friedrich, and S. Blügel, Quasiparticle band structure of the almost-gapless transition-metal-based Heusler semiconductor Si, Phys. Rev. B **93**, 195155 (2016).

[69] P. Haas, F. Tran, and P. Blaha, Calculation of the lattice constant of solids with semilocal functionals, Phys. Rev. B **79**, 085104 (2009).

[70] G. Stollhoff, A. M. Oleś, and V. Heine, Stoner exchange interaction in transition metals, Phys. Rev. B **41**, 7028 (1990).

[71] E. Şaşıoğlu, I. Galanakis, C. Friedrich, and S. Blügel, Ab initio calculation of the effective on-site Coulomb interaction parameters for half-metallic magnets, Phys. Rev. B **88**, 134402 (2013).

[72] H. A. Dürr, G. van der Laan, D. Spanke, F. U. Hillebrecht, and N. B. Brookes, Electron-correlation-induced magnetic order of ultrathin Mn films, Phys. Rev. B **56**, 8156 (1997).

[73] M. Pajda, J. Kudrnovsky, I. Turek, V. Drchal, and P. Bruno, Ab initio calculations of exchange interactions, spin-wave stiffness constants, and Curie temperatures of Fe, Co, and Ni, Phys. Rev. B **64**, 174402 (2001).

[74] E. Şaşıoğlu, L. M. Sandratskii, P. Bruno, and I. Galanakis, Exchange interactions and temperature dependence of magnetization in half-metallic Heusler alloys, Phys. Rev. B **72**, 184415 (2005).

[75] L. M. Sandratskii, E. Şaşıoğlu, and P. Bruno, Exchange interactions and Néel temperature of a Fe monolayer on W(001): A first-principles study, Phys. Rev. B **73**, 014430 (2006).

[76] I. Galanakis, M. Alouani, and H. Dreyssé, Interface magnetism in ultrathin Fe/W(110) films from first principles, Phys. Rev. B **62**, 3923 (2000).